Aalto University

OPEN ACCESS

This is an electronic reprint of the original article.
This reprint may differ from the original in pagination and typographic detail.

Flora, Bableen; Kumar, Rohit; Tiwari, Preeti; Kumar, Akhilesh; Ruokolainen, Janne; Narasimhan, Ashwin Kumar; Kesari, Kavindra Kumar; Gupta, Piyush Kumar; Singh, Anjuvan

Development of chemically synthesized hydroxyapatite composite with reduced graphene oxide for enhanced mechanical properties

Published in:
Journal of the Mechanical Behavior of Biomedical Materials

DOI:
10.1016/j.jmbbm.2023.105845

Published: 01/06/2023

Document Version
Publisher's PDF, also known as Version of record

Published under the following license:
CC BY

Please cite the original version:
Flora, B., Kumar, R., Tiwari, P., Kumar, A., Ruokolainen, J., Narasimhan, A. K., Kesari, K. K., Gupta, P. K., & Singh, A. (2023). Development of chemically synthesized hydroxyapatite composite with reduced graphene oxide for enhanced mechanical properties. *Journal of the Mechanical Behavior of Biomedical Materials*, *142*, 1-10. Article 105845. https://doi.org/10.1016/j.jmbbm.2023.105845

This material is protected by copyright and other intellectual property rights, and duplication or sale of all or part of any of the repository collections is not permitted, except that material may be duplicated by you for your research use or educational purposes in electronic or print form. You must obtain permission for any other use. Electronic or print copies may not be offered, whether for sale or otherwise to anyone who is not an authorised user.

journal of the mechanical behavior of biomedical materials 142 (2023) 105845

Contents lists available at ScienceDirect

Journal of the Mechanical Behavior of Biomedical Materials

journal homepage: www.elsevier.com/locate/jmbbm

Development of chemically synthesized hydroxyapatite composite with reduced graphene oxide for enhanced mechanical properties

Bableen Flora [a], Rohit Kumar [b], Preeti Tiwari [c], Akhilesh Kumar [d], Janne Ruokolainen [e], Ashwin Kumar Narasimhan [f], Kavindra Kumar Kesari [e,g,*], Piyush Kumar Gupta [b,h,i,**], Anjuvan Singh [a,***]

[a] Department of Biotechnology, School of Bioengineering and Biosciences, Lovely Professional University, Phagwara, Punjab, India
[b] Department of Life Sciences, Sharda School of Basic Sciences and Research, Sharda University, Greater Noida, 201310, Uttar Pradesh, India
[c] Centre for Interdisciplinary Research in Basic Science, Jamia Millia Islamia, Jamia Nagar, New Delhi, 110025, India
[d] Division of Medicine, ICAR-Indian Veterinary Research Institute Izatnagar, Bareilly, 243122, Uttar Pradesh, India
[e] Department of Applied Physics, School of Science, Aalto University, Espoo, 00076, Finland
[f] Advanced Nano-Theranostics (ANTs), Biomaterials Lab, Department of Biomedical Engineering, SRM Institute of Science and Technology, Kattankulathur, Tamil Nadu, 603203, India
[g] Faculty of Biological and Environmental Sciences, University of Helsinki, Biocenter 3, Helsinki, Finland
[h] Department of Life Sciences, Graphic Era (Deemed to be University), Dehradun, 248002, Uttarakhand, India
[i] Faculty of Health and Life Sciences, INTI International University, Nilai, 71800, Malaysia

ARTICLE INFO

Keywords:
Reduced graphene oxide
Hydroxyapatite
Calcination
Mechanical strength
Surface roughness

ABSTRACT

A successful attempt has been made to improve the mechanical properties of Hydroxyapatite (HAp) and reduced graphene oxide (rGO) composite nanoparticles (NPs). Various proportions of HAp and rGO were synthesized to improve the mechanical properties. HAp NPs were prepared using the wet precipitation method and further calcined to form crystalline particles. The physicochemical characterization of the HAp NPs revealed that the crystalline size and percentage of crystallinity were calculated to be 42.49 ± 1.2 nm and 44% post calcination. Furthermore, the rGO-HA composites were prepared using ball milling and obtained in the shape of pellets with different ratios of rGO (10, 20, 30, 40, 50% wt.). The mechanical properties have been evaluated through a Universal testing machine. Compared to calcined HAp (cHAp), the strength of variants significantly enhanced with the increased concentration of rGO. The compressive strength of HA-rGO with the ratio of the concentration of 60:40% by weight is a maximum of about 10.39 ± 0.43 MPa. However, the porosity has also been bolstered by increasing the concentration of rGO, which has been evaluated through the liquid displacement method. The mean surface roughness of the composites has also been evaluated from the images through Image J (an image analysis program).

1. Introduction

The global market for biomaterials has been reported to be bolstered at the rate of 15.4% from 2022 to 2030, and Orthopedic implant is the largest biomaterial market. Thereupon health risk, including osteoarthritis, osteoporosis, and musculoskeletal disorders, craves artful research for orthopedic implants. Nevertheless, other health issues, such as diabetes and obesity, strongly affect bone density (Oudrhiri et al., 2019). Although various metallic bone implants, including Titanium and Stainless Steel, have become the gold standards for bone imperfections, surgical and biomimetic constraints weaken the approach. Numerous materials such as polymers, metals, ceramics, and their composites are being fabricated through different techniques targeting bone regeneration and replacement (Gobbi, 2019; Kim et al., 2020). Lyons and

* Corresponding author. Department of Applied Physics, School of Science, Aalto University, Espoo, 00076, Finland.
** Corresponding author. Department of Life Sciences, Sharda School of Basic Sciences and Research, Sharda University, Greater Noida, 201310, Uttar Pradesh, India.
*** Corresponding author. Department of Biotechnology, School of Bioengineering and Biosciences, Lovely Professional University, Phagwara, Punjab, India.
E-mail addresses: kavindra.kesari@aalto.fi, kavindra.kesari@helsinki.fi (K.K. Kesari), piyush.kumar1@sharda.ac.in, dr.piyushkgupta@gmail.com (P.K. Gupta), anjuvan@gmail.com, anjuvan.15950@lpu.co.in (A. Singh).

https://doi.org/10.1016/j.jmbbm.2023.105845
Received 11 February 2023; Received in revised form 3 April 2023; Accepted 8 April 2023
Available online 9 April 2023
1751-6161/© 2023 The Authors. Published by Elsevier Ltd. This is an open access article under the CC BY license (http://creativecommons.org/licenses/by/4.0/).

Table 1
Percentage of HAp and rGO used for different blends.

Blends	HAp (%)	rGO (%)
cHAp	100	0
HrG1	90	10
HrG2	80	20
HrG3	70	30
HrG4	60	40
HrG5	50	50

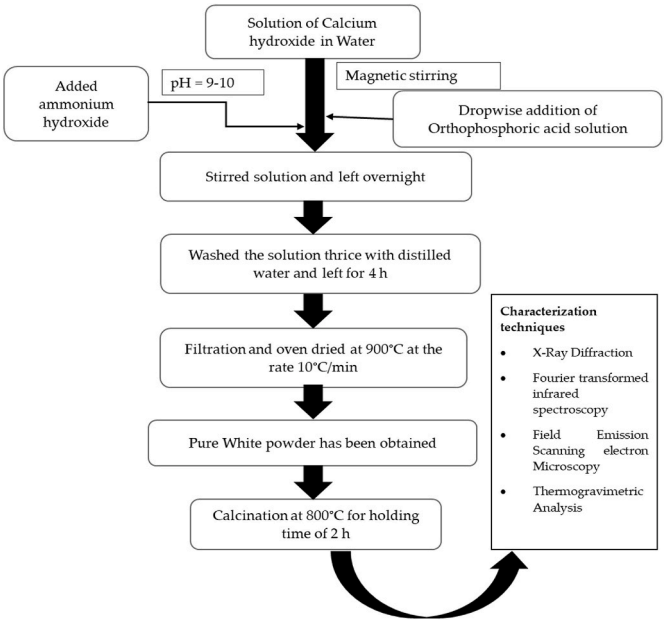

Fig. 1. Flowchart for the wet chemical synthesis of HAp.

coworkers confabulated the need for biomaterials along the composite fabrication to achieve the mechanically adaptable, biodegradable, and immunologically responsive bioimplant for bone regeneration (Lyons et al., 2020). Modifications in raw materials would improve the mechanical strength of the composite NPs. Sintering techniques can achieve this use of advanced fabrication methods, blending with appropriate polymer or metal to the ceramics to accomplish the need for autogenous bones (Kim et al., 2020; Nosrati et al., 2020a; Islam et al., 2019).

Despite many similarities with human bone, HAp material has been extensively used due to its biocompatibility and osteoconductive properties (Shin et al., 2015). However, the lower mechanical strength of the HAp as compared to the bone needs it to be blended with an appropriate material that aggravates its strength (Florea et al., 2020). Furthermore, carbon-based materials such as graphene and its oxides have also become another candidate to strengthen HAp. Graphene is made of sigma bonds between sp2 carbon atoms in a thick one-atom layer that add-ons its strength. The members of the graphene family, including GO and rGO, are the two essential materials that engrossed the interest of researchers.

Numerous sources and processes are available for synthesizing and rGO (Lesiak et al., 2021). The rGO possesses synonymous structural characteristics with the pristine graphene that augmented its strength compared to GO and diversified its application in membranes, catalysts, sensors, and supercapacitors (Hidayah et al., 2017a). Further, accelerated bone regeneration and enhanced osteogenesis have already been reported on MC3T3 cells (Lee et al., 2015). The composite of rGO (1.5%) and HAp has been investigated for mechanical behavior that showed increased elastic modulus (Nosrati et al., 2020a). Furthermore, a nanocomposite of HA/rGO has been fabricated using hot isostatic pressing (HIP). It has been reported to have enhanced biological and mechanical properties with increased rGO content (Baradaran et al., 2014). In addition, the rGO (0.25, 0.5,1, and 2% wt.) has been reinforced in HA and investigated for mechanical and biological behavior using MTT analysis. It has been concluded that the rGO-HA with 1% and 0.5% rGO showed biocompatibility on NIH-3T3 fibroblast cells and enhanced mechanical strength (Elif et al., 2017a).

Herein, we synthesized HAp using the wet precipitation method and incorporated it with rGO, prepared using GO through thermal reduction. The higher weight percentages of rGO (10, 20, 30, 40, and 50 % wt.) have been used to reinforce HAp, which has not been reported to date. In addition, to fabricate the composites with different concentrations ball milling method has been implemented, and the mechanical strength of the variants has been enhanced using the thermal method. The HA/rGO composite's strength and morphology have been studied precisely on

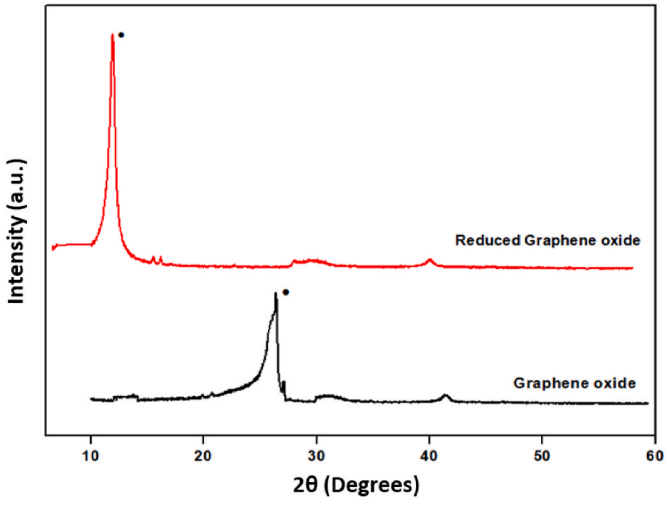

Fig. 3. XRD peaks for GO and rGO.

Fig. 2. Pellets of cHAp and rGO composites in a different ratio.

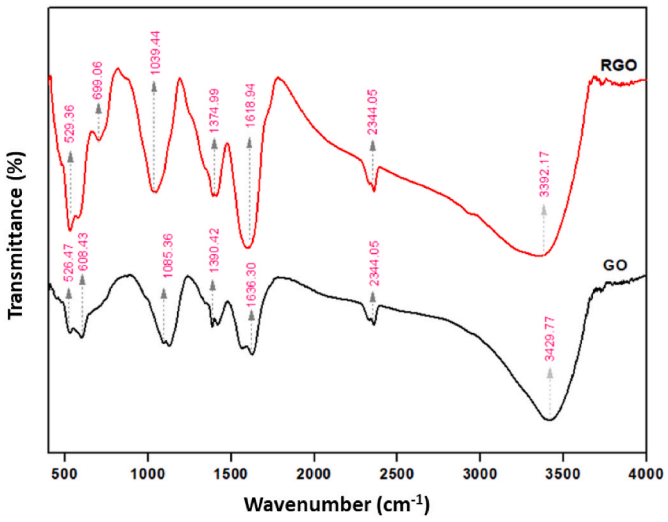

Fig. 4. FTIR analysis of GO and rGO.

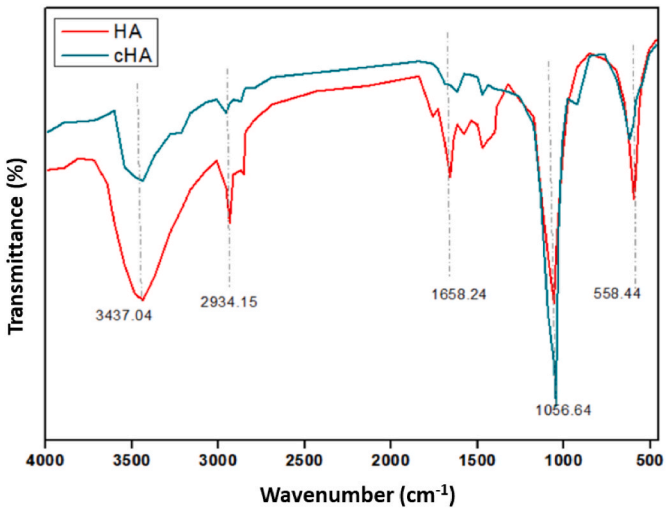

Fig. 5. FTIR analysis of HAp and cHAp.

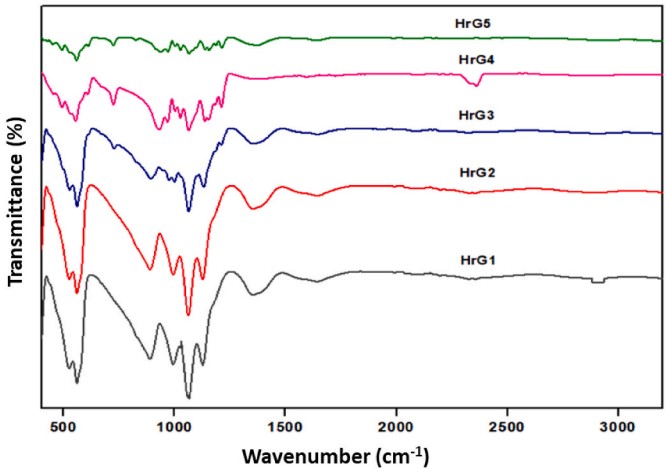

Fig. 6. FTIR Spectra of composites of HAp and rGO.

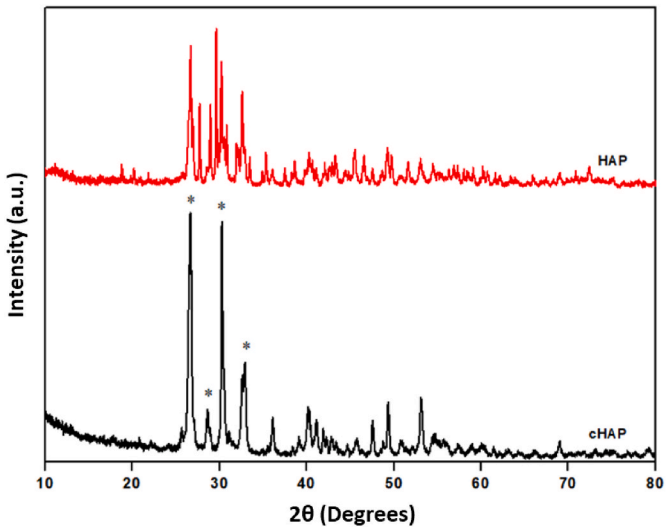

Fig. 7. XRD peaks of calcined cHAp and HAp.

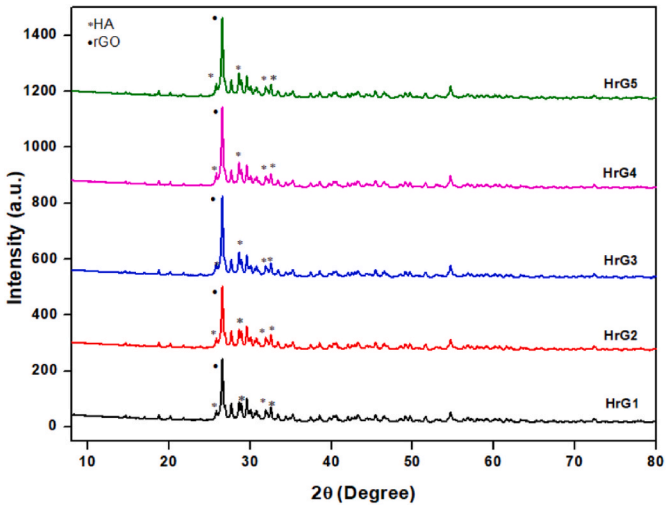

Fig. 8. XRD Peaks of variants of HAp and rGO.

Table 2
Spacing between the atoms in blends of HAp and rGO.

2 thetas	*d spacing(A°)*	hkl
25.7	0.171	(002)
31.8	0.211	(211)
32.5	0.215	(300)

the ball. In addition, the prepared HAp and rGO have been evaluated based on Fourier transform infrared spectroscopy (FTIR), Field Emission Scanning electron microscopy (FESEM), Thermogravimetric (TG) analysis, and X-ray powder diffraction (XRD) instruments. The mechanical strength of the composite has been determined by a Universal testing machine (UTM). The porosity has also been studied using the liquid displacement method. The novelty of this work is to produce the mechanically improved composite of HGA/rGO and study its characteristic features, including crystallinity, surface roughness, thermal behavior, and porosity, using different techniques. Nevertheless, the two-way ANOVA was performed on the compressive strength before and after thermal treatment. The purpose of the work was to achieve better mechanical strength, which has been successfully achieved.

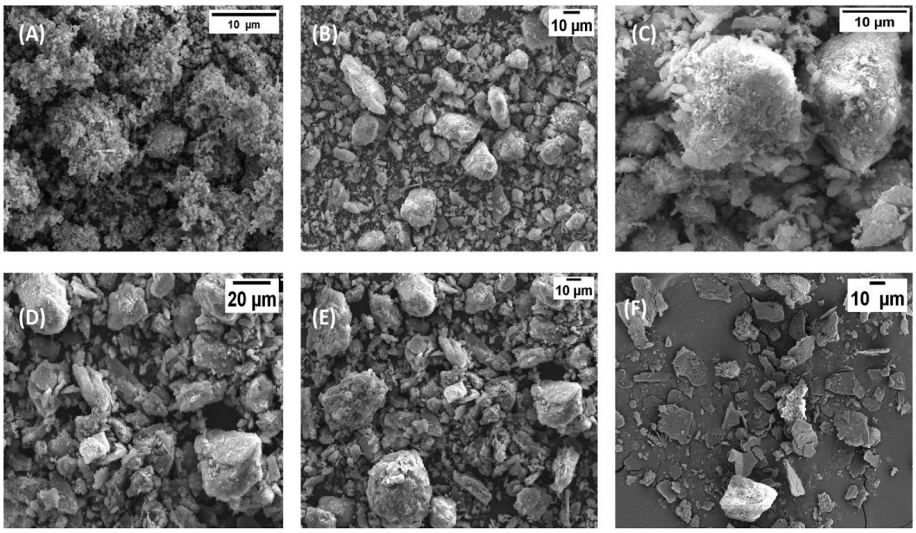

Fig. 9. FESEM images of the variants (A) CHA, (B) HrG1, (C) HrG2, (D) HrG3, (E) HrG4, and (F) HrG5.

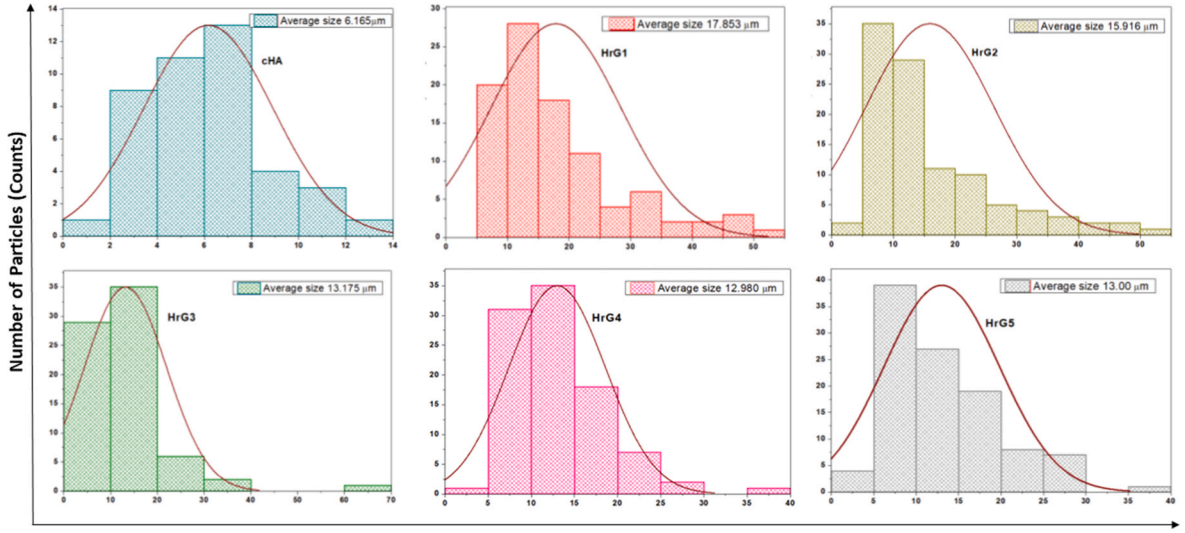

Fig. 10. Particle size analysis of the composites of HAp and rGO.

2. Materials and methods

2.1. Materials

High-purity GO powder with a bulk density of ~1.91 g/cc with solubility in water, calcium hydroxide, orthophosphoric acid, ammonium hydroxide, and other polar solvents were purchased from Sigma Aldrich.

2.2. Methods

2.2.1. Synthesis of HAp

HAp has been synthesized by mixing 10 M Calcium hydroxide Ca $(OH)_2$ in 500 mL and 6M orthophosphoric acid (H_3PO_4) prepared in 300 mL in an aqueous solution. The solution H_3PO_4 was added dropwise to Ca $(OH)_2$ upon magnetic stirring for 2 h.

$$10Ca(OH)2 + 6H3(PO4) \rightarrow Ca10(PO4)6\ (OH)2 + 18\ H2O \quad (1)$$

Add 1 M of ammonium hydroxide (NH_4OH) to the above mixture to maintain the basic pH under continuous stirring and stay undisturbed overnight. Then the solution was washed thrice with distilled water and left undisturbed for 4 h. Finally, the powder form of NPs was annealed at 900 °C at the rate of 10 °C/min. The final obtained powder was pure, white, and crystalline (Yelten and Yilmaz, 2016; Yelten-Yilmaz and Yilmaz, 2018).

2.2.2. Calcination of HAp

HAp showed improved physicochemical properties when subjected to calcination. Heat treatment improvises the material's crystallinity, and on calcination, the crystallinity is enhanced but limits the carbonate ion and porosity (Ahmed et al., 2015; Figueiredo et al., 2010). The calcination of HAp has been done at 800 °C for 2 h to improve its physicochemical properties.

2.2.3. Thermal reduction of GO

The reduction of GO not only amends its physicochemical properties but also increases its dispersive power and mechanical behavior. Numerous ways of obtaining a reduced form of GO have been scrutinized, including chemical (Mehrali et al., 2014), solvothermal, photocatalysis (Pei and Cheng, 2012), and thermal reduction methods. GO's thermal reduction under different atmospheres, including air and nitrogen, has been reported (Le et al., 2018). The thermally rGO has been

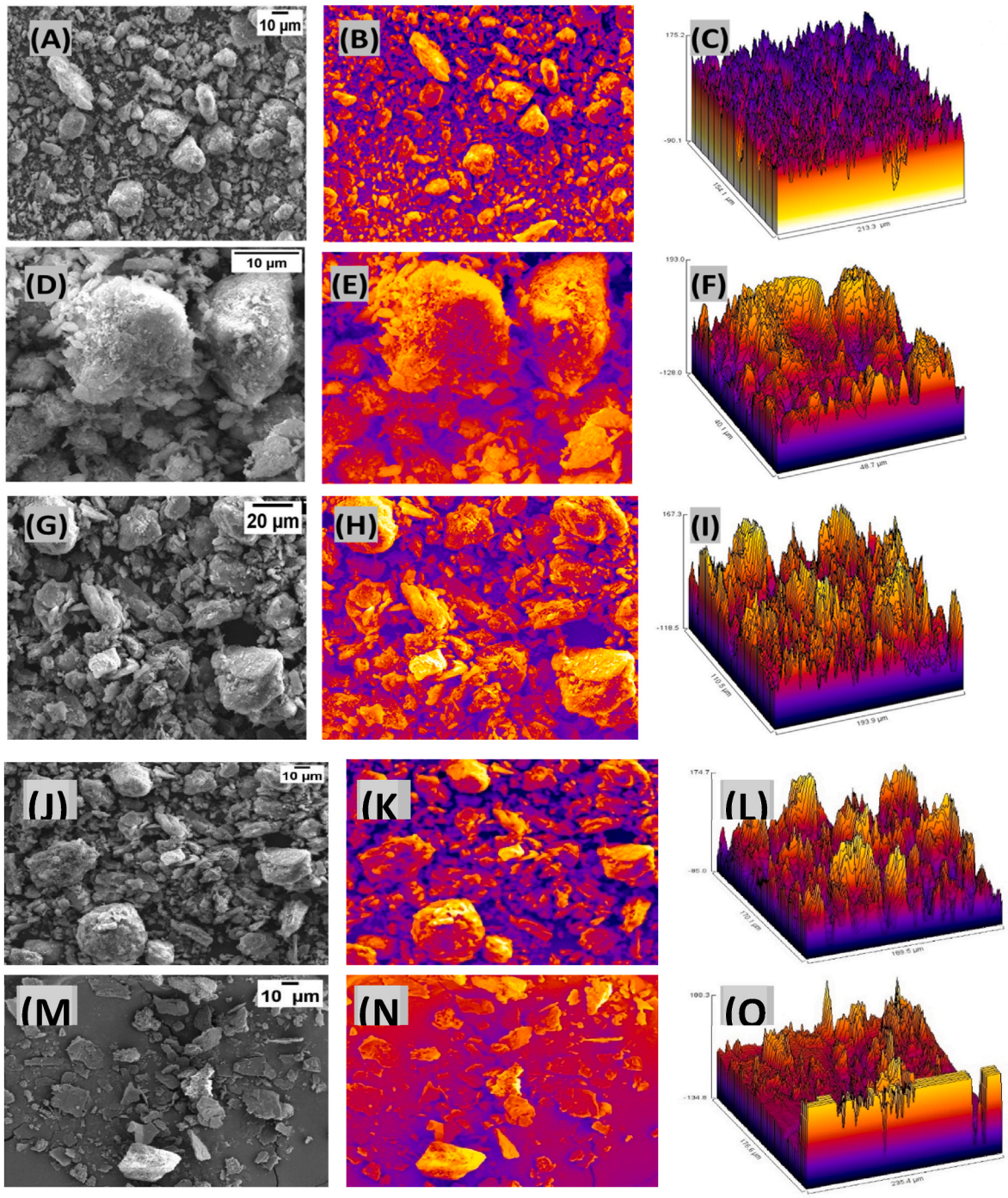

Fig. 11. Surface roughness (A–C) HrG1, (D–F) HrG2, (G–I) HrG3, (J–L) HrG4, and (M–O) HrG5.

Table 3
Roughness means and RMS values of blends of HAp and rGO.

Blends	Arithmetic Mean Roughness (Ra)	RMS
HrG1	38.063 ± 0.90	46.46 ± 0.68
HrG2	37.739 ± 0.22	43.10 ± 0.16
HrG3	31.283 ± 0.59	36.98 ± 0.62
HrG4	28.141 ± 0.43	34.22 ± 0.93
HrG5	21.286 ± 0.98	27.92 ± 0.52

further characterized.

2.2.4. Synthesis of rGO-HAp composite

The cHAp was reinforced with different concentrations of rGO (10, 20, 30, 40, and 50% weight), as mentioned in Table 1. The powdered samples were fabricated using the ball impact process before and after heat treatment. The ball impact process was performed using 5 metal balls of 5 mm thickness that were vibrated along the blending powder using a vortex for 30 min. The powder was then subjected to high pressure of 5 tons for 30–60 s to make pellets through the KBr press machine. The pellets with a 4 mm thickness and diameter of around 15 mm were used further for the experimentation.

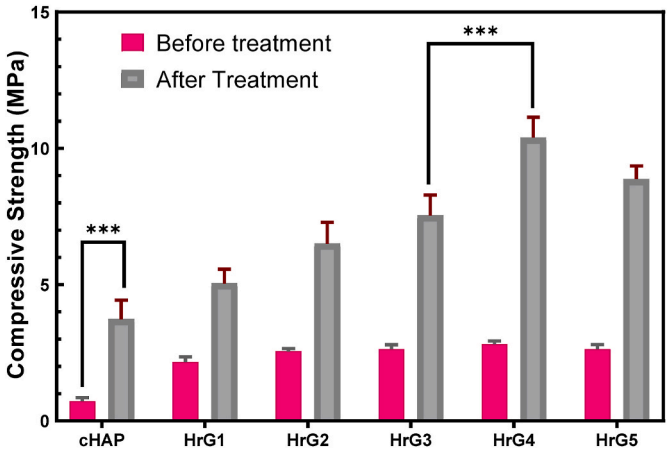

Fig. 12. Statistical analysis of compressive strength of composites before and after treatment *** indicates the $p < 0.0001$. All data were shown as mean value ± standard deviation.

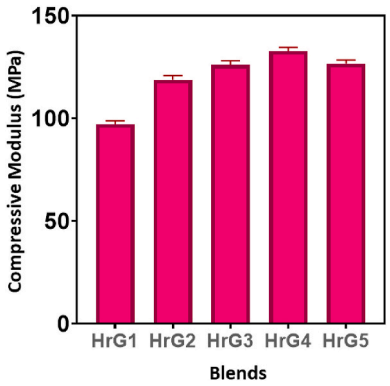

Fig. 13. The compressive modulus of variants of HAp and rGO.

Table 4
Toughness, Compressive modulus, and porosity of the composites of HAp and rGO.

Blends	Compressive Modulus (MPa)	Porosity %	Toughness
HrG1	97.21 ± 0.94	5.81 ± 0.41	12.26 ± 0.73
HrG2	118.81 ± 1.18	7.70 ± 0.60	18.24 ± 1.23
HrG3	126.13 ± 1.06	10.15 ± 0.53	22.90 ± 0.21
HrG4	132.73 ± 1.05	11.61 ± 0.44	39.41 ± 1.23
HrG5	126.67 ± 1.00	10.53 ± 0.65	36.80 ± 0.73

2.2.5. Physicochemical characterizations

Further, the prepared samples have been analyzed through Fourier transform infrared (FTIR) spectroscopy and X-ray diffraction (XRD) measurements. The scattering intensity in the X-ray diffraction techniques has been noted with the angles described as 2θ. The crystallinity of the sample has been evaluated through a Field emission scanning electron microscope (FESEM, JEOL EDS: OXFORD EDS LN2) equipped with energy-dispersive X-ray spectroscopy that allows the study of the surface morphology of the samples. The thermal analysis of the composite was studied using thermogravimetric analysis (TGA) at the heating rate of 10 °C/min rise in the temperature.

The compressive strength of calcined HA and rGO-HA composites has been evaluated through a Universal Testing machine (UTM). Composites were subjected to UTM to obtain the mechanical behavior with a crosshead speed of 5 mm min^{-1}. The pellets were made with a KBr Press machine with a radius of 0.66 cm and a height of 0.5 cm approx. The mechanical testing pattern was tested in triplicates for each variant at the rate of 5 mm min^{-1}. The comparative analysis of the mechanical strength of composite materials with and without heat treatment at 100 °C for 2 h was performed.

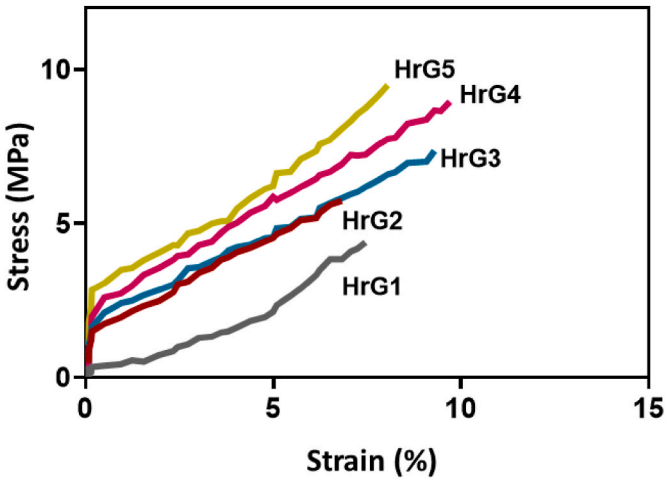

Fig. 14. Stress-strain graph for different blends of HAp and rGO.

2.2.6. Surface roughness and porosity of the composites

The surface roughness of the composite has been evaluated through FESEM using Image J. The root means square roughness (Rq), and the average roughness means (Ra) have been studied using the SurfCharJ plugin in Image J software. The surface plot has also been created to describe composites' roughness factor (Chinga et al., 2007). The porosity of the variants was measured by the Liquid displacement method. Briefly, the pellets with different compositions named HrG1, HrG2, HrG3, HrG4, HrG5, and cHA of equal dimensions of thickness of about 4 mm with a diameter 13 mm approximately measured with vernier Caliper were used to detect the percentage porosity after immersion in n-hexane for 30 min so that the pores can be occupied by the n-hexane (Chakraborty, Ponrasu, Chandel, Dixit, Muthuvijayan).

2.2.7. MTT assay

Cellular biocompatibility was explored by the MTT test which is based on the enzyme-dependent colorimetric test in which the reduction of a yellow-colored dye 3-(4-,5-dimethylthiazol-2yl)-2,5- diphenyltetrazolium bromide (MTT) into purple-colored formazan crystals occurs. This assay measures cellular viability. Precisely, after 72 h of incubation of Vero cells with composite material, the culture medium was removed from tested wells of the plate and replaced with MTT in DMEM media without serum proteins. Then the plates were incubated for 4 h at 37 °C, 5% CO_2. Later the culture medium was removed from each well and DMSO was added to dissolve the formazan crystal formed. Then the absorbance was recorded at 570 nm using an ELISA reader and the percentages of cell viability were calculated using the formula reported in an earlier study (Rodríguez-González et al., 2018).

2.2.8. Statistical analysis

The mechanical strength has been evaluated through Statistical analysis, which was performed using GraphPad. All variables were tested in triplets for each experiment, inclusive of before thermal treatment and after giving thermal treatment, and expressed as mean ± standard deviation (SD). On multiple comparisons, the maximum load-bearing capacity has been evaluated through two-way ANOVA analysis and Sidak's test.

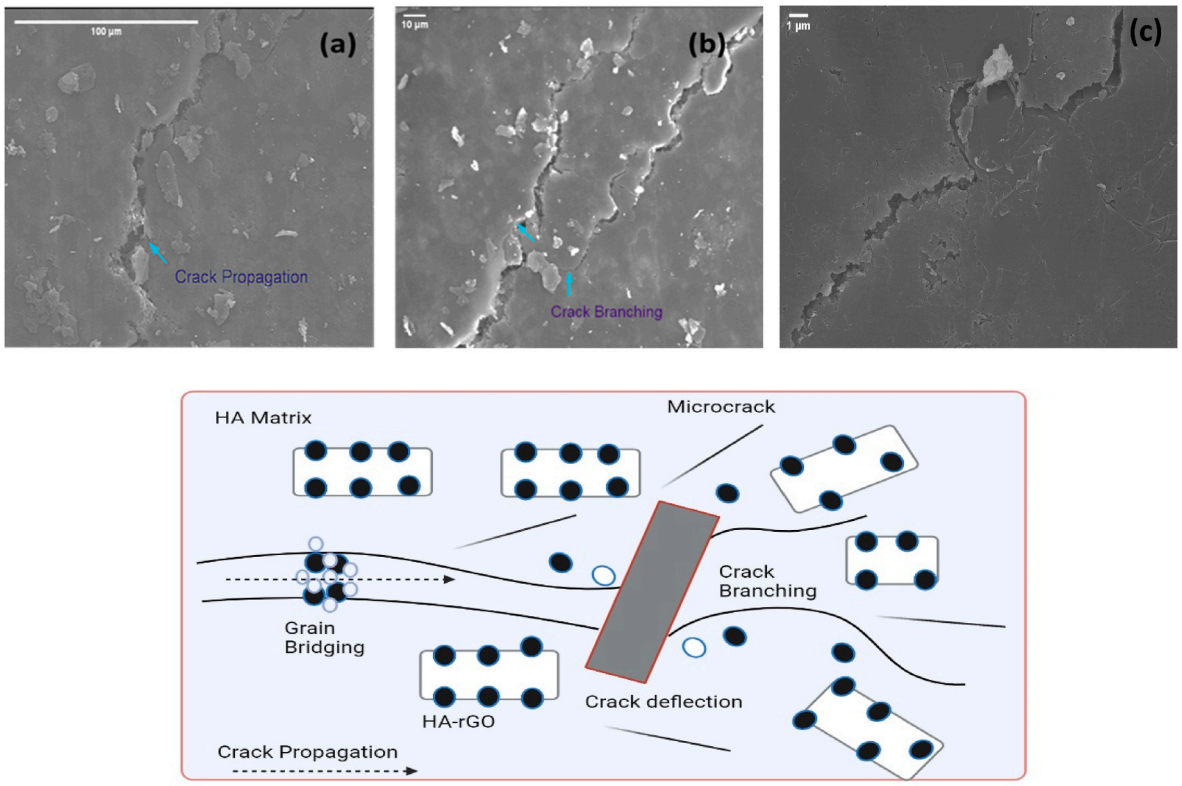

Fig. 15. FESEM images of HrG4 (a) Crack propagation at 100 μm, (b) Crack branching at 10 μm, (c) Crack deflection and the Crack propagation model.

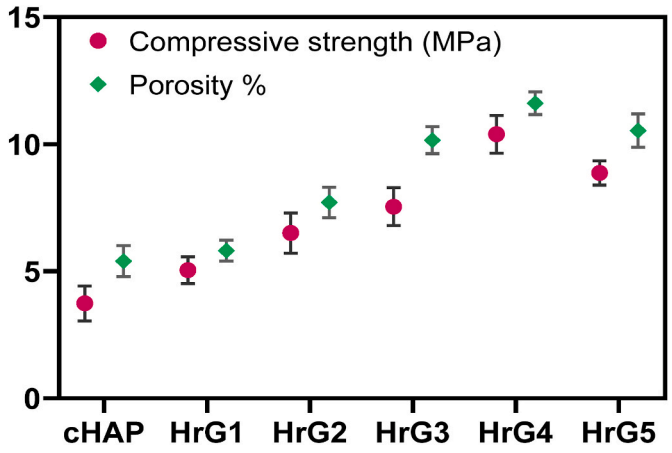

Fig. 16. Comparative analysis of compressive strength and porosity of different blends of HA/rGO.

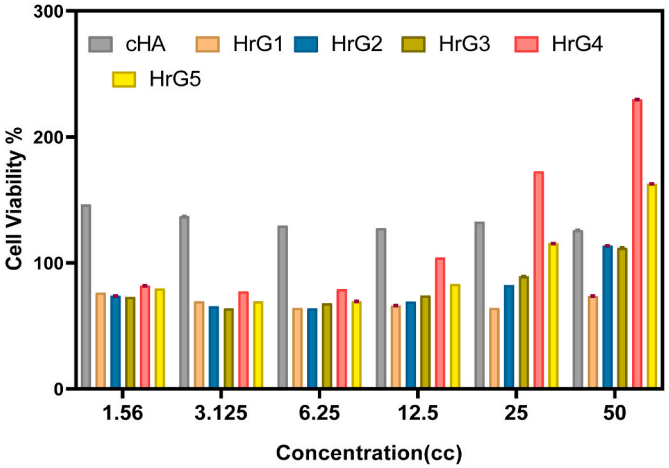

Fig. 17. Percentages of cell viability calculated in Vero cells for cHA and HAp and rGO composites (HrG1 to HrG5) after 72 h.

3. Results and discussion

3.1. Synthesis of rGO-HAp composite

HAp has been successfully prepared by the wet precipitation method, and a white crystalline powder has been obtained. The precipitates obtained have been characterized through XRD and FTIR analysis. In addition, it is then calcined at 800 °C to increase its crystallinity, confirmed by XRD analysis. On the other hand, the thermal reduction of GO has been carried out at a temperature of 200 °C for 1 h and has been scrutinized through FTIR and XRD analysis.

The preparation of HAp by chemical precipitation route and its characterization study is represented in Fig. 1. The pellet forms of different blends of HAp and rGO are shown in Fig. 2. The material has been shaped using the pellets-making machine with approximately 13 mm diameter and 3–5 mm thickness. Calcined HAp showed whitish pellets, whereas the color of the pellets became darker on increasing the concentration of rGO.

3.2. Physicochemical characterizations

The chemically synthesized HAp, cHAp, GO, and rGO have been investigated through FTIR and XRD. The FT-IR spectroscopy was performed within a wavelength range of 450–4000 cm^{-1} at room temperature. The diffraction pattern was analyzed through an XRD machine with a Cu-Kα source of radiations at the wavelength of 1.540. The diffraction was performed at 2θ values ranging from 0° to 95°.

3.2.1. X-ray diffraction (XRD) analysis of GO and rGO

The reduction of GO is confirmed through an X-ray diffraction analyzer. XRD pattern reveals the GO are polycrystalline structure. The XRD plot of GO showed a sharp peak at 11.8° with an interlayer distance of 0.733 nm, which corresponds to (002) hkl values, and on comparison with rGO, the peak corresponding to (002) found at 26.35° with an interlayer spacing of 0.334 nm. The cutback in d spacing values revealed the loss of water molecules and oxygen-containing groups and also in good tuning with the reported data by Alam and co-workers (Alam et al., 2017). Also, in rGO, the disappearance of the peak at 11.8° indicates that the oxygen-containing groups have been successfully eliminated shown in Fig. 3. The peaks observed in rGO correspond to JCPDS file no. 75–2078 also indicates the graphite phase of rGO.

3.2.2. FTIR analysis of GO and rGO

The FTIR for the GO and rGO has been studied. The reduction of GO has been achieved thermally. Fig. 4 reveals the FTIR spectroscopy patterns of GO and rGO. The functional groups present in both the GO and rGO can be analyzed through FTIR analysis. The comparative spectra of GO and rGO have been evaluated and the broad peak has been observed in the range of 3200–3500 cm^{-1} contributing to the O–H bond. In addition, other peaks were obtained at 2344 cm^{-1} and 1636 cm^{-1}, attributing to C═O stretching vibrations of carbonyl and carboxyl functional groups. Furthermore, a sharp peak for GO was obtained at 1095 cm^{-1} revealing vibrations of the C–O epoxy group. In the case of rGO, the intensity of oxygen-containing group vibration has been reduced including 1618.94 cm^{-1}, 2344 $cm^{-1,}$ and 1039 cm^{-1} concluding that the oxygen content has been reduced due to thermal treatment (Hidayah et al., 2017b; Muniyalakshmi et al., 2020).

3.2.3. FTIR analysis of HAp and cHAp

Structural analysis of cHAp was studied using FTIR. The different functional groups present in cHAp are shown in Fig. 5. The peaks at 558.44 cm^{-1} and 1056.64 cm^{-1} observed the vibrational stretching mode of the phosphate group in HAp. The peak at 1658.24 cm^{-1} is attributed to the carbonate group's stretching mode. Furthermore, the peak at 3437 cm^{-1} contributed to absorbed water (Ahmed et al., 2015; Alshemary et al., 2018). The FTIR spectra for all the other variants of HAp and rGO have been shown in Fig. 6.

3.2.4. XRD analysis of HAp and cHAp

The cHAp has been compared with the HAp studied through X-ray peaks in Fig. 7. The XRD pattern reveals the crystalline phase identification and crystallite size measured using the Scherrer equation and followed the standard JCPDS file no. 090432 observed in Fig. 7 (Ramesh et al., 2016). The calcination of HAp has been done at 800 °C, increasing the crystallinity, which can be observed in the XRD shown in Fig. 7. The XRD spectra for variants of HAp and rGO have been shown in Fig. 8. The blending can be observed clearly from the peaks. The characteristic peaks for HAp and rGO have been shown. The peak at 26.5 showed the characteristic peak of rGO that also overlaps with the peak of HAp. The characteristic peaks of HAp include peaks at $2\Theta = 25.7,28.7,31.8$, and 32.8, marked in the figure showing the successful formation of the composite of HAp and rGO as different variants. The d spacing and hkl values of the characteristic peaks have been determined through Bragg's law and tabulated in Table 2 (Nosrati et al., 2020b).

The crystallinity of the sample has been determined using the following formula:

$$C\% = \frac{Ac}{Ac + Aa} \times 100 \quad (2)$$

Where C% is the crystallinity percentage, Ac is the area of crystalline peaks, Aa denotes the area of all the amorphous and crystalline peaks. The percentage crystallinity of cHAp was found to be 42.49 ± 1.2. The increased crystallinity showed an improved mechanical strength on the addition of filler i.e., rGO, and the results have been shown in Fig. 11.

3.3. Morphological analysis of composite

The morphology of the variants of HAp and rGO have been characterized through FESEM images. Fig. 9 shows the FESEM images of the blend HrG1 to HrG4. The particle size analysis has also been done to evaluate the size of the variants through images using image J. On analysis, it has been observed that these are microparticles, and the particle size decreases with the increased concentration of rGO. Nevertheless, the maximum particle size obtained for HrG4 of about 12.980 μm, and the particle size of HrG1 of about 17.850 μm. The particle size plot is shown in Fig. 10.

3.4. Surface roughness studies of the composites

Surface roughness is a vital factor controlling cell adhesion and proliferation. Researchers reported that the cellular functions were impelled by surface roughness. For instance, Kunzler and coworkers found that osteoblast proliferation improved by increasing the surface roughness. But many studies showed that the roughness enhanced cellular proliferation and showed inconsistent behavior in evaluating in vitro studies (Faia-Torres et al., 2014; Kunzler et al., 2007; Rausch-fan et al., 2008). On the other hand, the proliferation of osteoblast MG-63 shrinked on increasing the surface roughness (Andrukhov et al., 2016). The surface roughness for the HAp and rGO variants has been reported in the Table below, which showed that the surface roughness decreases on increasing the concentration of rGO and a range of Ra values from 38.063 ± 0.90 to 27.286 ± 0.98 have been observed on analysis of the FESEM images using image J shown in Table 3. The roughness plot, as well as the images, have been shown in Fig. 11. As per the MTT evaluation, this has been observed that downturn in the surface roughness of the blends boosted the cell adhesion and proliferation can be clearly visualized in Fig. 17.

3.5. Mechanical testing of HAp/rGO composite

The compressive strength was determined for cHAp-rGO composites in different variations. A dramatic improvement in compressive strength was observed, except in HrG5, which showed mechanical strength 8.87 ± 0.27 MPa lower than HrG4. The highest mechanical strength was observed in HrG4, 10.39 ± 0.43 MPa. It can be concluded that the increased crystallinity on calcination of HAp and the removal of extra water content on reduction of GO enhances the interactions between the molecules, thereby increasing the compressive strength (Elif et al., 2017b). It has been observed on giving the thermal treatment to the pellets before mechanical analysis, the strength of the material ameliorated shown in Fig. 12.

The strength of the variants was facilitated by elevating the concentration of rGO in HAp up to 40%. In contrast, the strength declined slightly upon further increasing the rGO concentration, which can be observed in HrG5. Furthermore, it was studied that the strength increases on giving thermal treatment to the composites. The compressive modulus of various blends has been shown in Fig. 13 as well as represented in Table 4.

The findings validate that the mechanical behavior of the composite improved with the addition of rGO and through the way of its fabrication by giving thermal treatment. A stress-strain plot for each variant has also been shown in Fig. 14. A more significant stress-to-strain ratio was observed in the case of HrG4 responsible for the highest modulus achieved.

The crack analysis of the blend HrG4 has been done. Fig. 15 shows the way of development of cracks as well the development of its branches. The FESEM images were obtained after compression testing using the universal testing machine. After the ultimate strength, any rise in force being applied to the blend resulted in the development of cracks.

The development of the crack branching can also be observed in the figure, which witnessed the deviation of force applied without complete breakage. The crack branching conveys the resistance of the composite against the load being applied, validating the maximum compressive strength and modulus obtained for the HrG4 blend of HAp and rGO. The crack propagation model showed the crack deflection to different angles leads to branching as well as the grain bridging at some parts of the crack is in good tuning with the ceramics-based mechanism. Pulling out has not been observed at all (Feng et al., 2023; Shuai et al., 2021, 2022; Nosrati et al., 2020c).

3.6. Porosity of the composite

The porosity percentage of the composite was calculated using the mentioned formula:

$$Porosity\ \% = \frac{Was - Wbs}{\rho \quad V}\ 100 \tag{4}$$

Where Was is the weight of the pellets after soaking in n-hexane for 30 min and Wbs is the weight of the pellets before soaking in n-hexane, ρ is the density of n-hexane is 0.655 g/cc, and V is the volume of the pellets being used. The experiment was performed in triplicates (Nie et al., 2017). As the weight percentage of rGO increased, the porosity was reasonably compliant with the already reported HAp/rGO composite data. It is reasoned that the growth of HAp crystals was inhibited by rGO particles resulting in pore formation, hence elevating the porosity (Wang et al., 2021).

A comparative analysis of porosity and compressive strength showed that although the porosity gradually increases if the composite is gardened with rGO, the compressive strength and modulus are bolstered. This validates that rGO being reinforced to HAp improves its mechanical strength (Nosrati et al., 2020b; Zhou et al., 2019). Henceforth, a collateral relation between compressive strength and porosity has been observed as both declined slightly in the HrG5 composite, as shown in Table 4 and Fig. 16. Toughness corresponds to the area under the curve. It has been observed that the toughness increases by augmenting the concentration of rGO up to 40%. In contrast, it gets lowered on the further increasing concentration of rGO.

3.7. Cell viability analysis

Cytotoxicity was performed by MTT test on Vero cells. The cells were cultured in DMEM with 10% FBS, 4 mM of L-glutamine, and 4 mM of sodium pyruvate. The powdered form of HAp and rGO blends were added into 96-well plates and incubated the treated cells for 72 h. The different concentrations per cubic centimeter (cc) of each variant and cHAp have been used. It can be seen that on increasing the concentration of rGO from HrG1 to HrG5 the cell viability increases. Furthermore, by increasing the concentration of the powdered blends, the cell viability increases by increasing the concentration of variants (Nosrati et al., 2020c). In comparison with cHAp, the cellular compatibility ameliorated in HAp and rGO composites. The maximum cytocompatibility has been shown in HrG4 in Fig. 17.

4. Conclusion

In summary, HAp has been successfully prepared using the wet precipitation method and increased its crystallinity on calcination. Ball milling and pellets formation has been implemented to form variants of HA/rGO. The preparation of HAp and reduction of GO have been studied using X-ray diffraction, Fourier-transformed infrared spectroscopy, and Field Emission Scanning Electron microscope. Nevertheless, the porosity has also been evaluated through the liquid displacement method, and it determined that the porosity increased by increasing the concentration of rGO. However, the mechanical strength also increased the weight % of rGO in HA. Biocompatibility of the cHAp and rGO has been evaluated through MTT assay.

Furthermore, on giving the thermal treatment, a significant increase of about 50% in mechanical strength has been observed in HrG4 compared to cHA. However, the surface roughness has also been evaluated through image J, and the arithmetic mean of surface roughness (Ra) was found to be 27.83 ± 2.38 for HrG4, which has the highest compressive modulus of 132.73 ± 1.00 MPa, approximately. It also has been concluded that the strength of the HA-rGO blend increases by increasing the rGO content up to 40% due to decreasing particle size and thermal treatment provided to the pellets. Still, it gets lowered by further increasing the rGO concentration. Additionally, the biocompatibility of the variants of cHAp and rGO augmented on increasing the concentration of filler and in comparison to cHAp.

Compliance with ethics requirements

This article does not contain any studies with human or animal subjects.

CRediT authorship contribution statement

Bableen Flora: Writing – review & editing, Writing – original draft, Validation, Software, Methodology, Investigation, Data curation, Conceptualization. **Rohit Kumar:** Writing – review & editing, Data curation. **Preeti Tiwari:** Formal analysis, Investigation, Writing – review & editing. **Akhilesh Kumar:** Formal analysis, Investigation, Writing – review & editing. **Janne Ruokolainen:** Writing – review & editing, Visualization, Supervision. **Ashwin Kumar Narasimhan:** Writing – review & editing, Data curation. **Kavindra Kumar Kesari:** Writing – review & editing, Visualization, Validation, Supervision, Resources, Project administration, Funding acquisition. **Piyush Kumar Gupta:** Writing – review & editing, Visualization, Validation, Resources, Project administration. **Anjuvan Singh:** Writing – review & editing, Writing – original draft, Visualization, Validation, Supervision, Resources, Project administration, Methodology, Investigation, Formal analysis, Data curation, Conceptualization.

Declaration of competing interest

The authors declare that they have no known competing financial interests or personal relationships that could have appeared to influence the work reported in this paper.

Data availability

Data will be made available on request.

References

Ahmed, Y.M.Z., El-Sheikh, S.M., Zaki, Z.I., 2015. Changes in hydroxyapatite powder properties via heat treatment. Bull. Mater. Sci. 38 (7), 1807–1819. https://doi.org/10.1007/s12034-015-1047-0.

Alam, S.N., Sharma, N., Kumar, L., 2017. Synthesis of graphene oxide (GO) by modified hummers method and its thermal reduction to obtain reduced graphene oxide (RGO). Graphene 6 (1), 1–18. https://doi.org/10.4236/graphene.2017.61001.

Alshemary, A.Z., Akram, M., Taha, A., Tezcaner, A., Evis, Z., Hussain, R., 2018. Physicochemical and biological properties of hydroxyapatite extracted from chicken beaks. Mater. Lett. 215, 169–172. https://doi.org/10.1016/j.matlet.2017.12.076.

Andrukhov, O., Huber, R., Shi, B., Berner, S., Rausch-Fan, X., Moritz, A., Spencer, N.D., Schedle, A., 2016. Proliferation, behavior, and differentiation of osteoblasts on surfaces of different microroughness. Dent. Mater. 32 (11), 1374–1384. https://doi.org/10.1016/j.dental.2016.08.217.

Baradaran, S., Moghaddam, E., Basirun, W.J., Mehrali, M., Sookhakian, M., Hamdi, M., Moghaddam, M.R.N., Alias, Y., 2014. Mechanical properties and biomedical applications of a nanotube hydroxyapatite-reduced graphene oxide composite. Carbon 69, 32–45. https://doi.org/10.1016/j.carbon.2013.11.054.

Chakraborty, S.; Ponrasu, T.; Chandel, S.; Dixit, M.; Muthuvijayan, V. For Enhancing Angiogenesis in Tissue Engineering Applications. vol. 14.

Chinga, G., Johnsen, P.O., Dougherty, R., Berli, E.L., Walter, J., 2007. Quantification of the 3D microstructure of SC surfaces. J. Microsc. 227 (3), 254–265. https://doi.org/10.1111/j.1365-2818.2007.01809.x.

Elif, O., Belma, O., Ilkay, S., 2017a. Production of biologically safe and mechanically improved reduced graphene oxide/hydroxyapatite composites. Mater. Res. Express 4 (1), 015601. https://doi.org/10.1088/2053-1591/aa5464.

Elif, Ö., Belma, Ö., İlkay, Ş., 2017b. Production of biologically safe and mechanically improved reduced graphene oxide/hydroxyapatite composites. Mater. Res. Express 4 (1), 015601. https://doi.org/10.1088/2053-1591/aa5464.

Faia-Torres, A.B., Guimond-Lischer, S., Rottmar, M., Charnley, M., Goren, T., Maniura-Weber, K., Spencer, N.D., Reis, R.L., Textor, M., Neves, N.M., 2014. Differential regulation of osteogenic differentiation of stem cells on surface roughness gradients. Biomaterials 35 (33), 9023–9032. https://doi.org/10.1016/j.biomaterials.2014.07.015.

Feng, P., Shen, S., Yang, L., Kong, Y., Yang, S., Shuai, C., 2023. Vertical and uniform growth of MoS $_2$ nanosheets on GO nanosheets for efficient mechanical reinforcement in polymer scaffold. Virtual Phys. Prototyp. 18 (1), e2115384 https://doi.org/10.1080/17452759.2022.2115384.

Figueiredo, M., Fernando, A., Martins, G., Freitas, J., Judas, F., Figueiredo, H., 2010. Effect of the calcination temperature on the composition and microstructure of hydroxyapatite derived from human and animal bone. Ceram. Int. 36 (8), 2383–2393. https://doi.org/10.1016/j.ceramint.2010.07.016.

Florea, D.A., Chircov, C., Grumezescu, A.M., 2020. Hydroxyapatite particles—directing the cellular activity in bone regeneration processes: an up-to-date review. Appl. Sci. 10 (10), 3483. https://doi.org/10.3390/app10103483.

Gobbi, S.J., 2019. Requirements for selection/development of a biomaterial. BJSTR 14 (3). https://doi.org/10.26717/BJSTR.2019.14.002554.

Hidayah, N.M.S., Liu, W.-W., Lai, C.-W., Noriman, N.Z., Khe, C.-S., Hashim, U., Lee, H.C., 2017a. Comparison on Graphite, Graphene Oxide and Reduced Graphene Oxide: Synthesis and Characterization. Penang, Malaysia, 150002. https://doi.org/10.1063/1.5005764.

Hidayah, N.M.S., Liu, W.-W., Lai, C.-W., Noriman, N.Z., Khe, C.-S., Hashim, U., Lee, H.C., 2017b. Comparison on Graphite, Graphene Oxide and Reduced Graphene Oxide: Synthesis and Characterization. Penang, Malaysia, 150002. https://doi.org/10.1063/1.5005764.

Islam, Md S., Rahman, A.M.Z., Sharif, M.H., Khan, A., Abdulla-Al-Mamun, Md, Todo, M., 2019. Effects of compressive ratio and sintering temperature on mechanical properties of biocompatible collagen/hydroxyapatite composite scaffolds fabricated for bone tissue engineering. J. Asian Ceram. Soc. 7 (2), 183–198. https://doi.org/10.1080/21870764.2019.1600226.

Kim, T., See, C.W., Li, X., Zhu, D., 2020. Orthopedic implants and devices for bone fractures and defects: past, present and perspective. Eng. Regener. 1, 6–18. https://doi.org/10.1016/j.engreg.2020.05.003.

Kunzler, T.P., Drobek, T., Schuler, M., Spencer, N.D., 2007. Systematic study of osteoblast and fibroblast response to roughness by means of surface-morphology gradients. Biomaterials 28 (13), 2175–2182. https://doi.org/10.1016/j.biomaterials.2007.01.019.

Le, G.T.T., Manyam, J., Opaprakasit, P., Chanlek, N., Grisdanurak, N., Sreearunothai, P., 2018. Divergent mechanisms for thermal reduction of graphene oxide and their highly different ion affinities. Diam. Relat. Mater. 89, 246–256. https://doi.org/10.1016/j.diamond.2018.09.006.

Lee, J.H., Shin, Y.C., Lee, S.-M., Jin, O.S., Kang, S.H., Hong, S.W., Jeong, C.-M., Huh, J.B., Han, D.-W., 2015. Enhanced osteogenesis by reduced graphene oxide/hydroxyapatite nanocomposites. Sci. Rep. 5 (1), 18833 https://doi.org/10.1038/srep18833.

Lesiak, B., Trykowski, G., Tóth, J., Biniak, S., Kövér, L., Rangam, N., Stobinski, L., Malolepszy, A., 2021. Chemical and structural properties of reduced graphene oxide—dependence on the reducing agent. J. Mater. Sci. 56 (5), 3738–3754. https://doi.org/10.1007/s10853-020-05461-1.

Lyons, J.G., Plantz, M.A., Hsu, W.K., Hsu, E.L., Minardi, S., 2020. Nanostructured biomaterials for bone regeneration. Front. Bioeng. Biotechnol. 8, 922. https://doi.org/10.3389/fbioe.2020.00922.

Mehrali, M., Moghaddam, E., Shirazi, S.F.S., Baradaran, S., Mehrali, M., Latibari, S.T., Metselaar, H.S.C., Kadri, N.A., Zandi, K., Osman, N.A.A., 2014. Synthesis, mechanical properties, and in vitro biocompatibility with osteoblasts of calcium silicate–reduced graphene oxide composites. ACS Appl. Mater. Interfaces 6 (6), 3947–3962. https://doi.org/10.1021/am500845x.

Muniyalakshmi, M., Sethuraman, K., Silambarasan, D., 2020. Synthesis and characterization of graphene oxide nanosheets. Mater. Today: Proc. 21, 408–410. https://doi.org/10.1016/j.matpr.2019.06.375.

Nie, W., Peng, C., Zhou, X., Chen, L., Wang, W., Zhang, Y., Ma, P.X., He, C., 2017. Three-dimensional porous scaffold by self-assembly of reduced graphene oxide and nano-hydroxyapatite composites for bone tissue engineering. Carbon 116, 325–337. https://doi.org/10.1016/j.carbon.2017.02.013.

Nosrati, H., Sarraf-Mamoory, R., Zolfaghari Emameh, R., Aidun, A., Canillas Perez, M., 2020a. Enhancing mechanical properties of hydroxyapatite-reduced graphene oxide nanocomposites by increasing the spark plasma sintering temperature. Inorg. Nano-Metal Chem. 1–11 https://doi.org/10.1080/24701556.2020.1852251.

Nosrati, H., Sarraf-Mamoory, R., Zolfaghari Emameh, R., Le, D.Q.S., Canillas Perez, M., Bünger, C.E., 2020b. Low temperature consolidation of hydroxyapatite-reduced graphene oxide nano-structured powders. Mater. Adv. 1 (5), 1337–1346. https://doi.org/10.1039/D0MA00212G.

Nosrati, H., Sarraf-Mamoory, R., Kazemi, M.H., Canillas Perez, M., Shokrollahi, M., Zolfaghari Emameh, R., Falak, R., 2020c. Characterization of hydroxyapatite-reduced graphene oxide nanocomposites consolidated via high frequency induction heat sintering method. J. Asian Ceram. Soc. 8 (4), 1296–1309. https://doi.org/10.1080/21870764.2020.1842119.

Oudrhiri, M., Rherib, C., Oulja, M., Assermouh, A., Mahraoui, C., Hafidi, N.E., 2019. Requirements for selection/development of a biomaterial. BJSTR 14 (3), 1–6. https://doi.org/10.26717/BJSTR.2019.14.002554.

Pei, S., Cheng, H.-M., 2012. The reduction of graphene oxide. Carbon 50 (9), 3210–3228. https://doi.org/10.1016/j.carbon.2011.11.010.

Ramesh, S., Natasha, A.N., Tan, C.Y., Bang, L.T., Ramesh, S., Ching, C.Y., Chandran, H., 2016. Direct conversion of eggshell to hydroxyapatite ceramic by a sintering method. Ceram. Int. 42 (6), 7824–7829. https://doi.org/10.1016/j.ceramint.2016.02.015.

Rausch-fan, X., Qu, Z., Wieland, M., Matejka, M., Schedle, A., 2008. Differentiation and cytokine synthesis of human alveolar osteoblasts compared to osteoblast-like cells (MG63) in response to Titanium surfaces. Dent. Mater. 24 (1), 102–110. https://doi.org/10.1016/j.dental.2007.03.001.

Rodríguez-González, C., Salas, P., López-Marín, L.M., Millán-Chiu, B., De La Rosa, E., 2018. Hydrothermal synthesis of graphene oxide/multiform hydroxyapatite nanocomposite: its influence on cell cytotoxicity. Mater. Res. Express 5 (12), 125023. https://doi.org/10.1088/2053-1591/aae29c.

Shin, Y.C., Lee, J.H., Jin, O.S., Kang, S.H., Hong, S.W., Kim, B., Park, J.-C., Han, D.-W., 2015. Synergistic effects of reduced graphene oxide and hydroxyapatite on osteogenic differentiation of MC3T3-E1 preosteoblasts. Carbon 95, 1051–1060. https://doi.org/10.1016/j.carbon.2015.09.028.

Shuai, C., Yang, W., Feng, P., Peng, S., Pan, H., 2021. Accelerated degradation of HAP/PLLA bone scaffold by PGA blending facilitates bioactivity and osteoconductivity. Bioact. Mater. 6 (2), 490–502. https://doi.org/10.1016/j.bioactmat.2020.09.001.

Shuai, C., Peng, B., Feng, P., Yu, L., Lai, R., Min, A., 2022. In situ synthesis of hydroxyapatite nanorods on graphene oxide nanosheets and their reinforcement in biopolymer scaffold. J. Adv. Res. 35, 13–24. https://doi.org/10.1016/j.jare.2021.03.009.

Wang, B.-Y., Hsu, S., Chou, C.-M., Wu, T.-I., Hsiao, V.K.S., 2021. Improved mechanical properties of ultra-high shear force mixed reduced graphene oxide/hydroxyapatite nanocomposite produced using spark plasma sintering. Nanomaterials 11 (4), 986. https://doi.org/10.3390/nano11040986.

Yelten, A., Yilmaz, S., 2016. Various parameters affecting the synthesis of the hydroxyapatite powders by the wet chemical precipitation technique. Mater. Today: Proc. 3 (9), 2869–2876. https://doi.org/10.1016/j.matpr.2016.07.006.

Yelten-Yilmaz, A., Yilmaz, S., 2018. Wet chemical precipitation synthesis of hydroxyapatite (HA) powders. Ceram. Int. 44 (8), 9703–9710. https://doi.org/10.1016/j.ceramint.2018.02.201.

Zhou, K., Yu, P., Shi, X., Ling, T., Zeng, W., Chen, A., Yang, W., Zhou, Z., 2019. Hierarchically porous hydroxyapatite hybrid scaffold incorporated with reduced graphene oxide for rapid bone ingrowth and repair. ACS Nano 13 (8), 9595–9606. https://doi.org/10.1021/acsnano.9b04723.